Rare Metal Materials and Engineering
Volume 50, Issue 6, June 2021
Available online at www.rmme.ac.cn

Science Press

Cite this article as: Yao Huai, Xiong Yi, Zha Xiaoqin, et al. Microstructures, Mechanical Properties and Corrosion Behavior of Solution-Treated Mg-0.5Zr-1.8Zn-*x*Gd Biodegradable Alloys[J]. Rare Metal Materials and Engineering, 2021, 50(06): 1919-1927.

ARTICLE

Microstructures, Mechanical Properties and Corrosion Behavior of Solution-Treated Mg-0.5Zr-1.8Zn-*x*Gd Biodegradable Alloys

Yao Huai[1,2], Xiong Yi[1,2], Zha Xiaoqin[3], Li Huan[1], Shi Huina[1], Liu Ya[1]

[1] School of Materials Science and Engineering, Henan University of Science and Technology, Luoyang 471023, China; [2] Collaborative Innovation Center of Nonferrous Metals of Henan Province, Luoyang 471023, China; [3] Luoyang Ship Material Research Institute, Luoyang 471000, China

Abstract: The microstructure, mechanical and anticorrosion properties of Mg-0.5Zr-1.8Zn-*x*Gd (*x*=0, 0.5, 1.0, 1.5, 2.0, 2.5, wt%) alloys were investigated after a solution treatment at 470 ℃ for 10 h. Results indicate that the grain size of the alloy decreases with increasing the Gd content in the range of 0wt%~2.5wt%. When the Gd content is less than 1.5wt%, the alloy elements are more completely dissolved into the alloy matrix, and the second phase is mainly composed of nanoscale $(Mg, Zn)_3Gd$ precipitated particle. At the range of 1.5wt%~2.5wt%, the insoluble micron-scale $(Mg, Zn)_3Gd$ phase emerges in the alloy, and the number and size of the $(Mg, Zn)_3Gd$ phase increase with the Gd content. The Mg-0.5Zr-1.8Zn-1.5Gd alloy shows excellent mechanical properties and anticorrosive ability, which can be attributed to a more homogeneous microstructure and the presence of nanometric secondary phase particles. In the 120 h immersion experiment, the average corrosion rate of the Mg-0.5Zr-1.8Zn-1.5Gd alloy deceases at first, then increases, and then decreases slowly. At last, with the increase of immersion time, it eventually becomes stable.

Key words: magnesium alloys; solution treatment; microstructure; mechanical properties; corrosion

Magnesium (Mg) alloys show potential application as biodegradable materials for orthopedic implants because of their good biocompatibility, mechanical properties and biodegradability in biological systems[1-3]. However, the high degradation rate of magnesium alloys is the main factor restricting their application as biological transplantation, which can greatly reduce the mechanical properties of the alloy in advance. At the same time, it is also easy to produce a vast hydrogen gas, resulting in alkalinity around the transplantation, leading to inflammation and affecting bone healing[2,4].

Multiple alloying element addition has been used in Mg alloys. The mechanical properties and corrosion resistance of magnesium alloys can be enhanced by adding suitable alloying elements. Zirconium (Zr), which is usually added to Mg alloys as a grain refiner, has also been shown to improve the strength and corrosion resistance. The content of Zr in biodegradable magnesium alloys should be less than 1wt% because excessive Zr (>1wt%) will be precipitated from Mg alloy, causing severe galvanic corrosion[5]. Zinc (Zn) is one of the major elements in the human body, and has the potential to further improve the mechanical and corrosion properties of magnesium[6]. Gadolinium (Gd), as a magnesium alloying element, is predominantly used for strengthening mechanical properties and improving corrosion resistance[7]. In vitro tests indicate that the Gd element has good tolerance for human umbilical cord perivascular cells and mouse macrophages, and the production of inflammatory markers is lower than that of other rare earth elements[8]. Recent studies have found that the addition of a small amount of Gd is helpful to diminish the number of cancer cells[9]. Many experimental alloys based on Mg-Zr-Zn-Gd systems have been developed, and their microstructure, mechanical and corrosion properties were investigated[10,11]. It has been reported in Ref. [12] that the

Received date: June 28, 2020
Foundation item: Education Department of Henan Province (20A430010); National Natural Science Foundation of China (U1804146)
Corresponding author: Yao Huai, Ph. D., Lecturer, School of Materials Science and Engineering, Henan University of Science and Technology, Luoyang 471023, P. R. China, Tel: 0086-379-64231269, E-mail: yaohuai@163.com

corrosion rate of the as-cast Mg-6Gd-0.5Zn-0.4Zr alloy after soaking in SBF for 120 h is approximately 0.45 mm/a. Zhang et al[13] developed an as-extruded Mg-11.3Gd-2.5Zn-0.7Zr alloy which exhibits good mechanical properties and corrosion resistance, and its ultimate tensile strength (UTS), yield strength (YS), elongation to failure (EL) and corrosion rate are 341 MPa, 281 MPa, 13.5% and 0.17 mm/a, respectively.

Paying attention to the mechanical properties as well as corrosion resistance of biological magnesium alloys is essential, while the bio-safety of the alloys should also be considered. Although Gd element shows low toxicity in short-term cytotoxicity studies, the content of Gd element in the above Mg-Zr-Zn-Gd series biological magnesium alloys is on the high side, according to the principle of "bio-safety"[8]. Herein, we designed Mg-0.5Zr-1.8Zn-*x*Gd (*x*=0, 0.5, 1.0, 1.5, 2.0, 2.5, wt%) biological magnesium alloys using the principle of microalloying. However, in order to eliminate the defects of coarse second phase, composition segregation and uneven microstructure in the as-cast alloy, and to further improve the comprehensive properties of the alloy, the effects of solid solution treatment on the microstructure, mechanical properties and corrosion resistance of Mg-0.5Zr-1.8Zn-*x*Gd alloys were studied, with special emphasis on the corrosion mechanisms. It is hoped that knowledge provided here will benefit general biological material design beyond inventions of the alloys and the preparation strategy.

1 Experiment

1.1 Materials preparation

Alloy ingots with a nominal composition of Mg-0.5Zr-1.8Zn-*x*Gd were prepared from pure Mg and Zn (99.9wt%), Mg-25wt% Zr, and Mg-20wt% Gd master alloys in electric induc-tion furnace under an anti-oxidizing flux protection[14], and then solution-treated at 470 ℃ for 10 h followed by water quenching at about 60 ℃. Hereafter, these solution treated Mg-0.5Zr-1.8Zn-*x*Gd (*x*=0, 0.5, 1.0, 1.5, 2.0, 2.5, wt%) alloys were marked as T0, T0.5, T1.0, T1.5, T2.0 and T2.5, respectively.

1.2 Microstructure determination and mechanical properties

The microstructures and composition of the samples were examined via optical microscopy (OM, OLYMPUS PMG3), scanning electronic microscopy (SEM, JSM-5610LV) equipped with an energy dispersive spectrometer (EDS, PHOENIX, EDAX) and transmission electron microscopy (TEM, JEM-2100).

The samples for tensile test were made into rod tensile specimens with a diameter of 5 mm and a gauge length of 25 mm. Tensile test was performed at room temperature with a tensile speed of 1 mm/min under AG-1250KN (SHIMADZU) machine.

1.3 Electrochemical and immersion corrosion

The electrochemical study was carried out using an electrochemical workstation (Autolab PGSTAT128N) at a scanning rate of 1 $mV \cdot s^{-1}$ and potential window of 250 mV below and 400 mV above the open circuit potential. A three-electrode cell was employed with graphite sheet as the counter electrode, saturated calomel electrode as the reference electrode, and the sample (Φ11.3 mm×10 mm) mounted in epoxy resin as the working electrode. The test was performed in simulated body fluid (SBF) at 37 ℃ under a water bath, and the composition of SBF was reported in Ref. [15].

The immersion tests were conducted in SBF at a constant temperature of 37 ℃ for mass-loss tests. The ratio of the SBF to exposed surface area was 30 mL:1 cm^2, and in order to keep the pH stable, the SBF was renewed every 8 h. The corrosion rate P_w (mm/a) was calculated using the following equation based on ASTM G31-72[16]:

$$P_w=87.6\Delta W/\rho At \quad (1)$$

where ΔW is the mass loss (mg), ρ is the density of the alloy (g/cm^3), A is the surface area exposed (cm^2), t is the total immersion time (h). Each record was averaged over three measurements.

2 Results

2.1 Microstructure

Fig. 1 shows optical micrographs of solution treated Mg-0.5Zr-1.8Zn-*x*Gd alloys. A homogeneous distribution of equiaxed grains is observed in the solution treated alloys. As the Gd content increases from 0wt% to 0.5wt%, 1.0wt%, 1.5wt%, 2.0wt%, and 2.5wt%, the average grain size significantly decreases from 247 μm to 170, 156, 123, 115 and 113 μm, respectively. In addition, when the content of Gd is less than 1.5wt%, the second phase in the original cast alloy is almost completely dissolved in the alloy matrix. When the content of Gd is more than 1.5wt%, the black second phase particles in the alloy begin to appear, and the number and size of the second phase particles increase with the increase of Gd content.

A magnification backscattered electron SEM image of T1.5 alloy and the corresponding EDS element maps are shown in Fig.2. From Fig.2a, the T1.5 alloy is mainly composed of the α-Mg matrix and a small amount of white micron particles (A and B), indicating that most eutectic phases have been dissolved in the matrix. The result of surface scanning (Fig.2b) shows that the tiny white particles (C and D) are Zr-rich sites, which have been also reported by Zhang[17]. The Zr-rich particles as heterogeneous nucleation sites can promote the nucleation of α-Mg grains and refine the matrix grains. It can also be seen from Fig. 2b~2d that the Zr, Zn and Gd alloying elements are better dissolved into the alloy matrix and evenly distributed after Mg-0.5Zr-1.8Zn-1.5Gd alloy is solution treated at 470 ℃ for 12 h.

To further understand the microstructure of the second phase in solution treated Mg-0.5Zr-1.8Zn-*x*Gd alloys, TEM observation was carried out, as shown in Fig. 3. In the T1.5 alloy, as shown in Fig. 3a, some nano-scale elliptical precipitates are distributed dispersively in the α-Mg matrix. EDS analysis (Fig. 3b) indicates that the chemical composition of

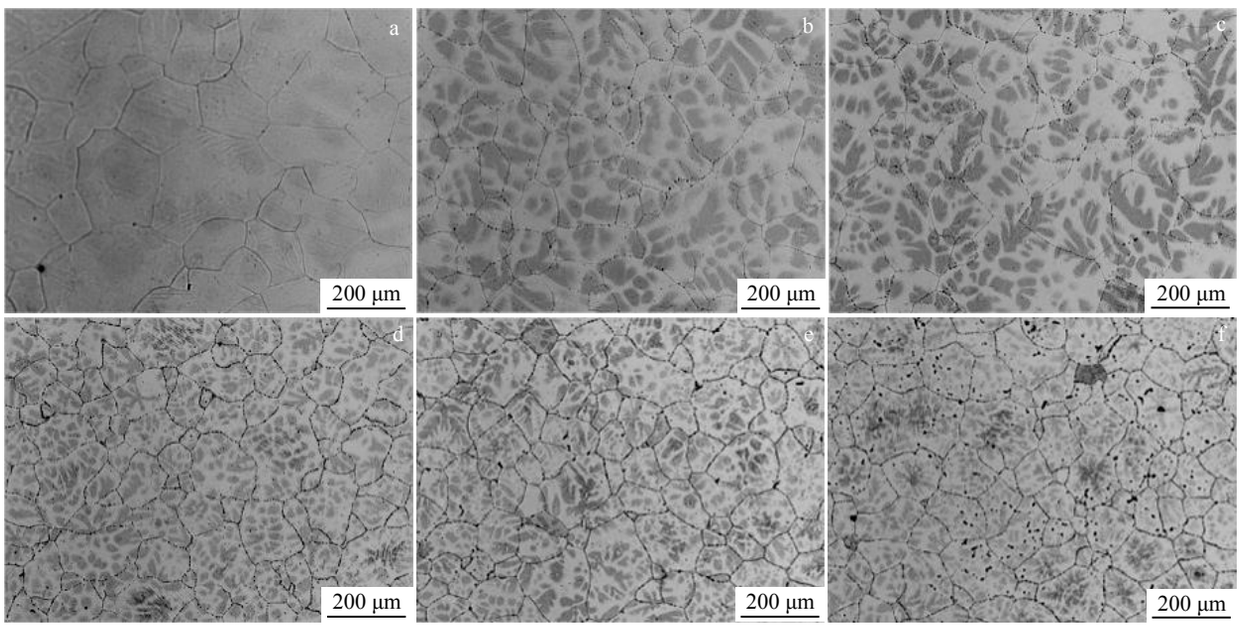

Fig.1 OM images of solution-treated Mg-0.5Zr-1.8Zn-*x*Gd alloys: (a) T0, (b) T0.5, (c) T1.0, (d) T1.5, (e) T2.0, and (f) T2.5

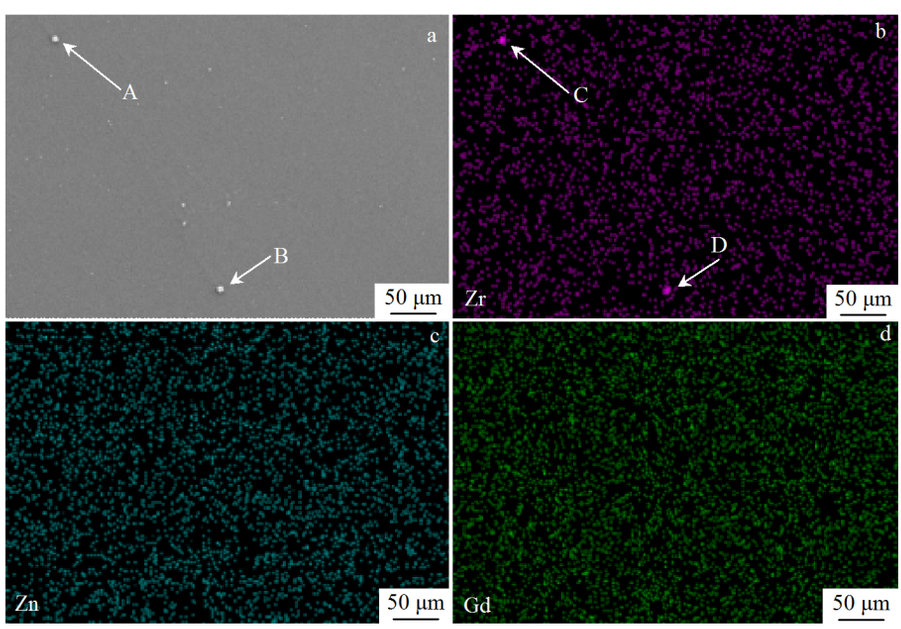

Fig.2 SEM image in backscattered electron mode (a) and corresponding EDS maps of Zr (b), Zn (c), and Gd (d) elements for T1.5 alloy

particle A mainly contains Mg, Zn and Gd elements. Particle A has a face-centered cubic (fcc) structure as given by the SAED determination in Fig. 3c. The interplanar spacing of SAED pattern in Fig. 3c is 0.4215, 0.1149 and 0.1227 nm, respectively, indexed to (111), (0$\bar{2}$6) and ($\bar{1}\bar{3}$5) planes of the Mg_3Gd. A lattice constant of a=0.7276 nm is observed along the [4$\bar{3}\bar{1}$] zone axis. As a result, it is recognized as the (Mg, Zn)$_3$Gd phase, and Zn atoms replace part of Mg atoms in the Mg_3Gd phase, resulting in the reduction of the standard lattice constant of the Mg_3Gd phase[18]. Fig. 3d and 3g are the TEM images of the T2.0 and T2.5 alloys, respectively. All second phases in the alloy are composed of micron-sized long strips and granules. It can be inferred that this second phase is caused by the incomplete dissolution of the larger size second phase from as-cast alloy during the solution process. The second phase of the B and C granular second phase in Fig. 3d and 3g was analyzed by EDS, and the second phase is all composed of Mg, Zn and Gd elements, as shown in Fig.3e and

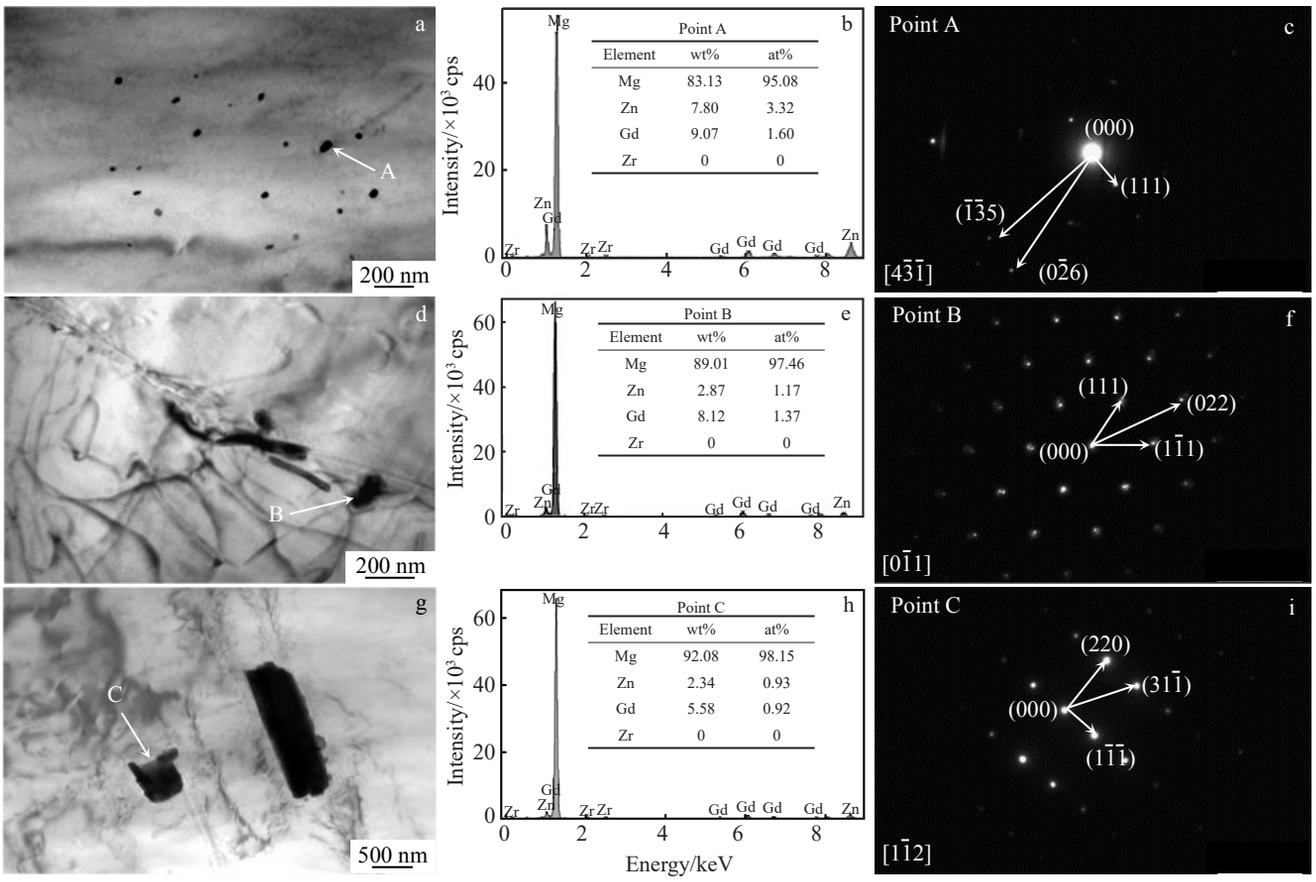

Fig.3 TEM images, EDS point analysis results and SAED patterns of the T1.5 (a~c), T2.0 (d~f) and T2.5 (g~i) alloys

3h. Fig. 3f and 3i show that the second phase particles in both alloys have face-centered cubic (fcc) structure. The interplanar spacing of 0.4218, 0.2578 and 0.4218 nm has a good correspondence to the (111), (022) and ($\bar{1}$11) crystal planes in the Mg_3Gd phase, respectively, with their axes parallel to the [0$\bar{1}$1] direction and a lattice parameter of 0.7301 nm (Fig. 3f). Meanwhile, the interplanar spacing of 0.4217, 0.2198 and 0.2577 nm has a good correspondence with the (1$\bar{1}\bar{1}$), (31$\bar{1}$) and (220) crystal planes in the Mg_3Gd phase, respectively, belonging to the [1$\bar{1}$2] crystal band axis with a lattice constant of 0.7294 nm (Fig. 3i). They are similar to the case of the T1.5 alloy. The second phases are grouped to $(Mg,Zn)_3Gd$ phase in both T2.0 and T2.5 alloys.

2.2 Mechanical properties

Fig.4 shows the engineering stress-strain curves of the solution treated Mg-0.5Zr-1.8Zn-*x*Gd alloys. And the corresponding UTS, YS and EL are listed in Table 1. Generally, the mechanical properties of the investigated alloys are improved with the Gd addition. The UTS, YS and EL increase first, then reach peak at 1.5wt%, and finally decrease. The T1.5 alloy owns the highest values of UTS (237±3 MPa), YS (177 ±3 MPa) and EL (12.5±0.4%).

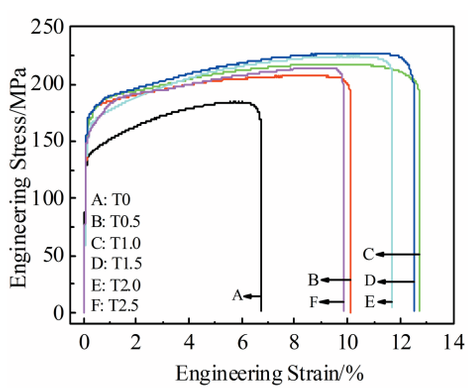

Fig.4 Engineering stress-strain curves of solution-treated Mg-0.5Zr-1.8Zn-*x*Gd alloys

Table 1 Mechanical properties of solution-treated Mg-0.5Zr-1.8Zn-*x*Gd alloys

Alloy	T0	T0.5	T1.0	T1.5	T2.0	T2.5
UTS/MPa	189±3	217±3	227±3	237±3	234±3	224±3
YS/MPa	137±3	159±3	169±3	177±3	172±3	164±3
EL/%	6.9±0.4	10.3±0.4	12.9±0.4	12.5±0.4	11.7±0.4	9.9±0.4

2.3 Fracture characteristics

Fig. 5 shows SEM fracture morphologies of the solution treated Mg-0.5Zr-1.8Zn-*x*Gd alloys. As shown in Fig.5a, when the content of Gd is 0, the fracture surface has obvious brittle fracture characteristics that cleavage surface perpendicular to the tensile direction and larger grain size appear in the fracture surface. Thus, the UYS, YS and EL of the alloy are low. When the Gd content is 0.5wt%, 1.0wt% and 1.5wt%, there are a large number of cleavage surfaces with different directions on the fracture surface in Fig. 5b~5d. A few small and shallow dimples appear in some fracture areas, and dimples increase with the increase of Gd content. The cleavage surface size gradually decreases with the increase of Gd content, belonging to the hybrid fracture feature. Therefore, the mechanical properties of the alloy gradually increase with the increase of Gd content. When the Gd content is 2.0wt% and 2.5wt%, the corresponding tensile fracture morphology is shown in Fig. 5e and 5f. The cleavage surface in the fracture surface is relatively flat, the area gradually increases, and the direction gradually tends to be consistent. The phenomenon is caused by the insoluble second phase with a large size in the alloy, which weakens the binding force of the grain boundary. Thus, the mechanical properties of the alloy decrease gradually with the increase of Gd content.

2.4 Polarization tests

The electrochemical polarization curves of the solution treated Mg-0.5Zr-1.8Zn-*x*Gd alloys are shown in Fig. 6. According to the open circuit potential measurement, the polarization curves are collected after stabilizing in SBF for 1 h. The corrosion potential (E_{corr}), corrosion current density (I_{corr}) and corrosion rate (P_i) values are derived directly from these curves by Tafel region extrapolation. The corresponding results are summed up in Table 2. As shown in Fig.6 and Table 2, the E_{corr} gradually transfers to positive directive, reaching its maximum at 1.5wt% of Gd, and then decreases. The tendency of I_{corr} and P_i are opposite to that of E_{corr}. From the viewpoint of thermodynamics, for the same kind of alloy, the more positive the E_{corr}, the lower tendency to self-corrosion for the alloy. From a kinetic point of view, lower I_{corr} and P_i indicate that the alloy is less susceptible to self-corrosion, meaning that the alloy has a lower corrosion rate. As previously mentioned, T1.5 alloy has better corrosion resistance[19].

2.5 Immersion tests

Fig. 7 shows that the corrosion rates for the solution treated Mg-0.5Zr-1.8Zn-*x*Gd alloys measured by mass loss after immersion for 120 h. The corrosion rates decrease gradually with the Gd addition from 0wt% to 1.5wt%, and then increase from 1.5wt% to 2.5wt%. The lowest corrosion rate of T1.5 alloy is determined to be 0.534±0.035 mm/a. A similar trend is found in the determination of corrosion rates measured through electrochemical and immersion methods.

Texture, grain size and second phase are the main factors influencing the corrosion behavior of Mg alloys [20]. When the Gd content is less than 1.5wt%, the corrosion rate of the alloys gradually decreases with the increase of the Gd content. It can be seen that when the Gd content is 0 (Fig. 1), the alloy has a larger grain size, leading to lower corrosion resistance in SBF[21]. The morphology of the alloy after corrosion (Fig. 8a) shows that the T0 alloy has relatively severe corrosion and exhibits a few large shallow corrosion pits. The appearance of

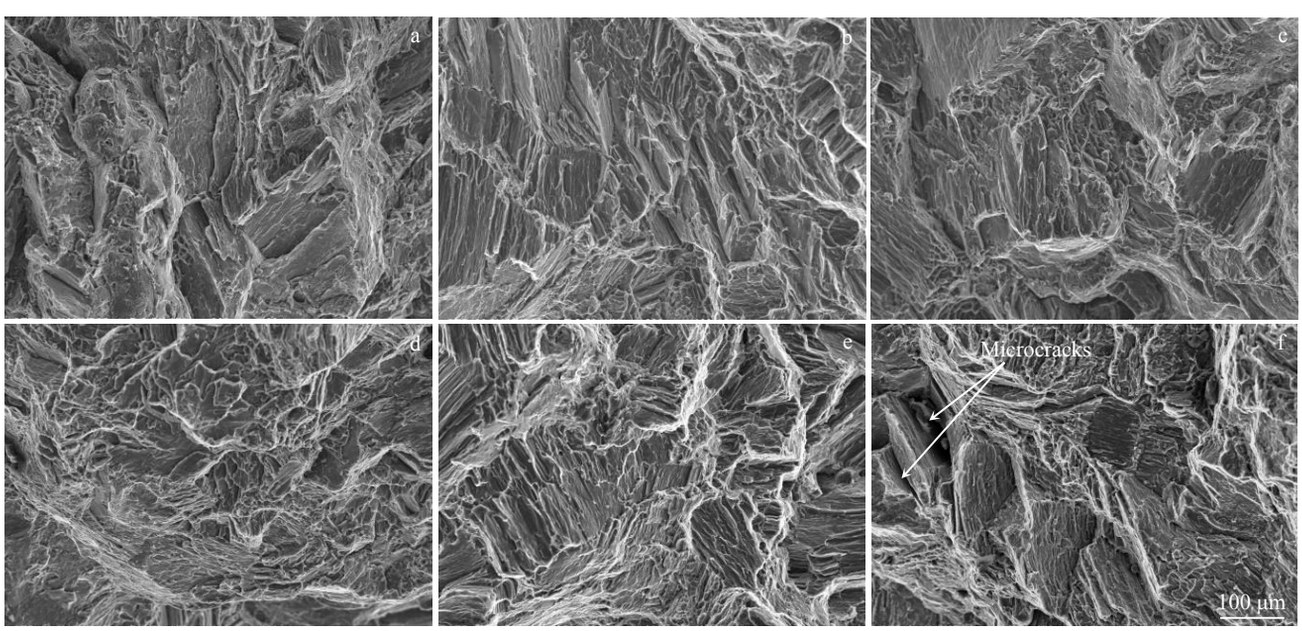

Fig.5 SEM morphologies of tensile fracture surface of solution-treated Mg-0.5Zr-1.8Zn-*x*Gd alloys: (a) T0, (b) T0.5, (c) T1.0, (d) T1.5, (e) T2.0, and (f) T2.5

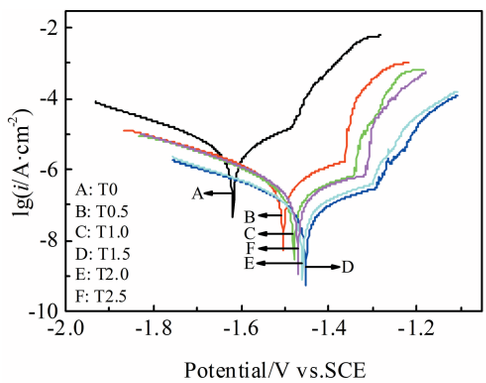

Fig.6 Polarization curves of solution-treated Mg-0.5Zr-1.8Zn-*x*Gd alloys immersed in SBF for 1 h

shallow corrosion pits is usually related to the distribution of uneven particle size within the alloy[22]. With increasing the Gd content, the grain size decreases and the corrosion resistance of the alloy gradually increases[23]. At the same time, as the alloying elements are dissolved in the alloy matrix, the E_{corr} of the alloy matrix gradually increases, and the corrosion resistance of the alloy is gradually enhanced[24]. Therefore, when the Gd content is less than 1.5wt%, the corrosion resistance of the alloy is gradually enhanced with the increase of the Gd content. The second phase in the as-cast Mg-Zr-Zn-Gd alloy is usually distributed in a continuous or semi-continuous network at the grain boundaries[25]. Therefore, the amount of alloying elements after solution treatment along the original grain boundaries into the grain gradually decreases, the corresponding self-corrosion potential gradually decreases, and the corrosion rate gradually increases. As

Table 2 E_{corr}, $I_{corr}$and P_i of solution-treated Mg-0.5Zr-1.8Zn-*x*Gd alloys derived from the polarization curves

Alloy	T0	T0.5	T1.0	T1.5	T2.0	T2.5
E_{corr}/V vs. SCE	-1.619±0.003	-1.505±0.003	-1.480±0.003	-1.453±0.003	-1.460±0.003	-1.470±0.003
I_{corr}/μA·cm^{-2}	9.248±0.004	5.608±0.005	4.049±0.005	3.562±0.005	3.577±0.005	3.718±0.004
P_i/mm·a^{-1}	0.414±0.003	0.252±0.003	0.183±0.004	0.161±0.004	0.162±0.003	0.169±0.003

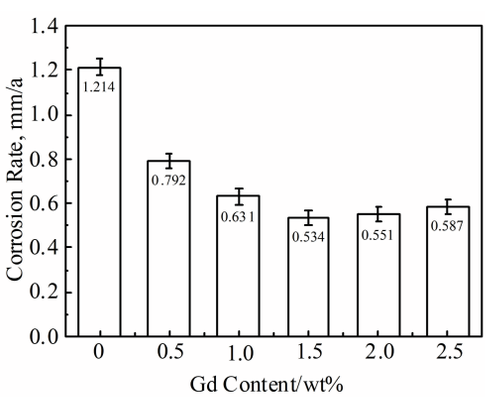

Fig.7 Corrosion rates for solution-treated Mg-0.5Zr-1.8Zn-*x*Gd alloys measured by mass loss after immersion for 120 h

shown in Fig. 8b~8f, the surface morphology of the Gd-containing alloys after corrosion are mainly composed of shallow honeycomb structures.

When the Gd content is more than 1.5wt%, as shown in Fig. 3d and 3g, the amount and size of the rest (Mg, Zn)$_3$Gd phase particles in the alloy gradually increase as the Gd content increases. The (Mg, Zn)$_3$Gd particles usually act as the cathode to accelerate the dissolution of the α-Mg matrix as the anode. Therefore, as the Gd content increases, the corrosion rate of the alloy gradually increases[26]. At the same time, the rapid dissolution of the α-Mg matrix as the anode will cause the (Mg, Zn)$_3$Gd phase particles as the cathode to fall off. As shown in Fig. 8e and 8f, larger size holes appear on the surface of the alloy after corrosion and the number and size of corrosion holes gradually increase with increasing the Gd content.

Fig. 9 shows the average corrosion rate of the T1.5 alloy within 120 h of immersion in the SBF every 8 h. From the diagram, it can be seen that the corrosion rate decreases first, then increases, then decreases slowly, and finally tends to stabilize with the increase of soaking time.

3 Discussion

In the as-cast Mg-0.5Zr-1.8Zn-*x*Gd alloy in this experiment, the second phase mainly exists as (Mg, Zn)$_3$Gd phase with different morphologies and sizes. Since the melting point of the second phase in the alloy is about 520 ℃, a solution temperature of 470 ℃ and a holding time of 10 h were chosen[27]. The grain size of as-cast Mg-Zr-Zn-Gd alloys gradually decreases with the increase of Gd content, while the amount and size of the second phase gradually increase with the increase of Gd content[28]. Therefore, as shown in Fig.1 and Fig. 3, under the same solid solution conditions, the grain size of the alloy gradually decreases with the increase of Gd content, and the amount and size of the undissolved second phase gradually increase with the increase of Gd content. When the Gd content is less than 1.5wt%, as shown in Fig. 2, the second phase in the alloy is thoroughly dissolved in the alloy matrix. When the Gd content is more than 1.5wt%, as shown in Fig. 3, there are a few undissolved second phases.

Generally, the mechanical properties of solution treated Mg-0.5Zr-1.8Zn-*x*Gd alloys at room temperature are mainly dependent on the grain size and the second phase characters, i. e. morphology, size and distribution. When the Gd content is less than 1.5wt%, it can be seen from Fig. 1 that with the increase of the Gd content, the grain size of the alloy gradually decreases. The grain refinement can improve the mechanical properties of the alloy according to the Hall-Petch

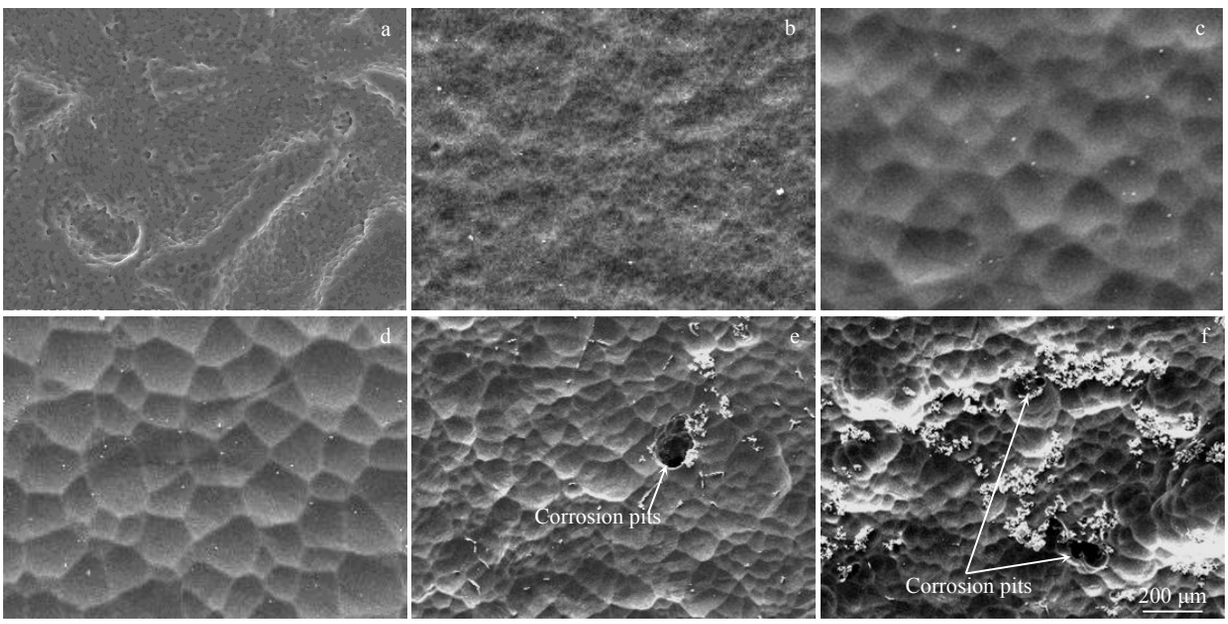

Fig.8 SEM morphologies of the corroded samples after immersion for 120 h and corrosion removal: (a) T0, (b) T0.5, (c) T1.0, (d) T1.5, (e) T2.0, and (f) T2.5

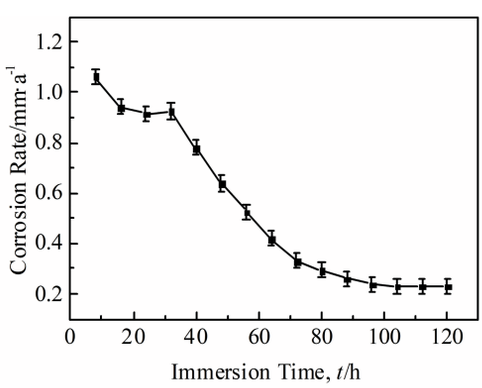

Fig.9 Corrosion rates for T1.5 alloy measured by mass loss every 8 h

equation[29]. At the same time, Fig. 2 and Fig. 3 show that the alloying elements are better dissolved in the alloy matrix, and alloying elements dissolved in the alloy matrix increase with the increase of the Gd content. The difference between Gd and Mg in atomic radius and valence makes Gd dissolved in the alloy matrix play a certain solid solution strengthening effect[30]. For alloys with the same composition, the solid solution strengthening effect is directly proportional to the concentration of the solute in the alloy[31]. Therefore, as the Gd content increases, the mechanical properties of the alloy gradually increase. As shown in Fig. 3a, a mass of nano-scale (Mg, Zn)$_3$Gd precipitates appear in the 1.5wt% Gd alloy. The nano-precipitated phase and the alloy matrix usually have a coherent or semi-coherent interface relationship. This interface relationship will better pin dislocations, increase the dislocation movement resistance, and play a better second phase strengthening effect [32]. When the Gd content is less than 1.5wt%, the amount of nano-scale (Mg, Zn)$_3$Gd precipitated phase in the alloy will increase with the increase of Gd content. Therefore, the mechanical properties of the alloy gradually increase with the increase of Gd content.

When the Gd content is more than 1.5wt%, the amount of alloying elements dissolved in the alloy matrix remains basically unchanged, and the solid solution strengthening effect of the alloying elements remains unchanged[33]. In Fig. 3d and 3g, there is undissolved (Mg, Zn)$_3$Gd phase with a large size in the alloy, which has a non-coherent interface relationship with the matrix. It is easy to generate a stress field at the interface between the second phase and the matrix, which reduces the mechanical properties of the alloy[32]. At the same time, as shown in Fig. 3f, under the action of tensile stress, the coarse (Mg, Zn)$_3$Gd phase region is easy to become the source of crack initiation and crack propagation channel. Consequently, the strength and ductility of the alloy decrease as the Gd content increases.

Combined with the microstructure of the T1.5 alloy, the morphology after corrosion and the change of corrosion rate in different periods, the corrosion model of the alloy was established. The corrosion model is shown in Fig. 10. According to the change of corrosion rate of T1.5 alloy in different time periods, the change of corrosion process is divided into three stages.

The first stage (0~24 h) is shown in Fig. 10a. At the beginning of immersion, the following reactions occur mainly on the surface of the alloy[34]:

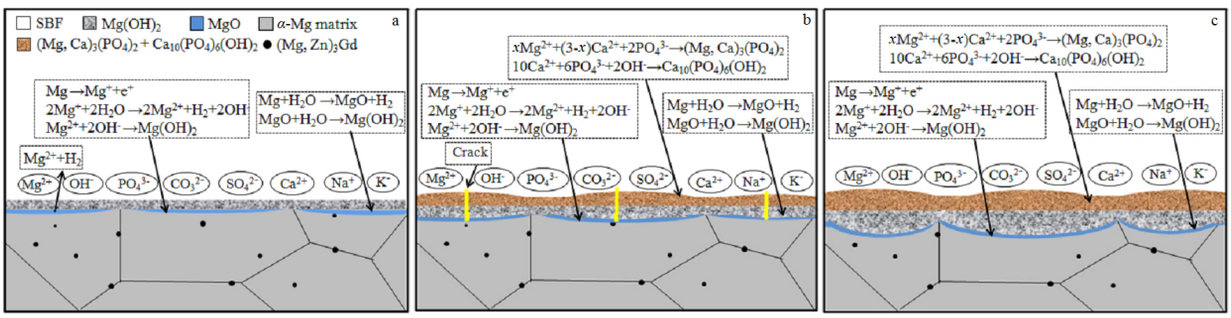

Fig.10 Corrosion behavior model of T1.5 alloy in SBF: (a) first stage; (b) second stage; (c) third stage

$$Mg \rightarrow Mg^{+}+e^{-} \quad (2)$$

$$2Mg+2H_2O \rightarrow 2Mg^{+}+H_2+2OH^{-} \quad (3)$$

$$Mg^{2+}+2OH^{-} \rightarrow Mg(OH)_2 \quad (4)$$

As the immersion time increases, the alloy surface is gradually covered by the corrosion product $Mg(OH)_2$, and the corrosion product is gradually thickened with the increase of immersion time, which leads to the decrease of the average corrosion rate. At the same time, the alloy surface will also produce a certain thickness of MgO film, and the following reaction occurs[34]:

$$Mg+H_2O \rightarrow MgO+H_2 \quad (5)$$

$$MgO+H_2O \rightarrow Mg(OH)_2 \quad (6)$$

The second stage (24~32 h) is shown in Fig. 10b. In this stage, with the gradual increase of the surface Mg^{2+} and OH^{-} concentration of the corrosion layer, the following reactions occur on the surface with the corrosion product of $Mg(OH)_2$ [35]:

$$xMg^{2+}+(3-x)Ca^{2+}+2PO_4^{3-} \rightarrow (Mg,Ca)_3(PO_4)_2 \quad (7)$$

$$10Ca^{2+}+6PO_4^{3-}+2OH^{-} \rightarrow Ca_{10}(PO_4)_6(OH)_2 \quad (8)$$

The resulting $Mg(OH)_2$, $(Ca, Mg)_3(PO_4)_2$ and $Ca_{10}(PO)_4(OH)_2$ corrosion products form a dense corrosion layer on the alloy surface. In the grain center region, the H_2 generated at a faster rate will lead to the rupture of the dense corrosion layer in this region and increase the contact area between the alloy surface and the SBF, resulting in an increase in the corrosion rate in this region, which accelerates the formation of dimples. At the same time, it also increases the average corrosion rate during this immersion period[36].

The third stage (32~120 h) is shown in Fig. 10c. When the immersion time is 32~96 h, with the increase of immersion time, the newly formed corrosion products lead to the gradual healing of cracks in the central region of the original grain, which reduces the contact area between the alloy and the SBF. At the same time, the corrosion products on the alloy surface will gradually increase with the increase of immersion time. Therefore, the corrosion rate of this stage gradually decreases with the increase of immersion time. When the soaking time is 96~120 h, the rate of forming corrosion products by SBF, the permeation of corrosion layer and the reaction of alloy gradually approach and tend to be consistent with the dissolution rate of corrosion products, that is, the corrosion products reach a dynamic equilibrium between formation and dissolution, resulting in stable corrosion with the immersion time[37].

4 Conclusions

1) Minor Gd addition can effectively refine the grain size, and change composition of second phase. The Mg-0.5Zr-1.8Zn-*x*Gd alloys mainly consist of the *α*-Mg and $(Mg, Zn)_3Gd$ phase. Many nano-scale $(Mg, Zn)_3Gd$ phases are precipitated in the alloy as the Gd content is less than 1.5wt%. There is a small amount of micron-scale insoluble $(Mg, Zn)_3Gd$ phase remaining in the alloy as the Gd content is above 1.5wt%, and its quantity and size increase with the increase of Gd content.

2) The UTS, YS, EL and corrosion resistance of the solution treated Mg-0.5Zr-1.8Zn-*x*Gd alloys increase with the Gd content increasing within the 0wt%~1.5wt% range, and then decrease within the range of 1.5wt%~2.5wt%. The UTS, YS, EL and corrosion rate of T1.5 alloy are 237±3 MPa, 177±3 MPa, 12.5±0.4%, and 0.534±0.035 mm/a, respectively.

3) The corrosion rate of T1.5 alloy in different immersion time intervals in SBF has obvious changes. Within 0~24 h, the corrosion rate decreases gradually with the increase of soaking time; within 24~32 h, the corrosion rate increases gradually with the increase of soaking time due to the local rupture of the corrosion layer; within 32~120 h, first of all, the newly formed corrosion products gradually heal the rupture of the corrosion layer, and at the same time it is continuously thickened, which leads to the gradual decrease of the corrosion rate with the increase of soaking time, and then the corrosion rate tends to stabilize when the corrosion products reach the dynamic equilibrium between formation and dissolution.

References

1 Mareci D, Bolat G, Izquierdo J *et al*. *Materials Science and Engineering C*[J], 2016, 60: 402

2 Liu Y X, Curioni M, Liu Z. *Electrochimica Acta*[J], 2018, 264: 101

3 Zhang Y, Li J Y, Liaw P K *et al*. *Journal of Alloys and Compounds*[J], 2018, 769: 552

4 Brooks E K, Der S, Ehrensberger M T. *Materials Science and Engineering C*[J], 2016, 60: 427

5 Zhang J S, Zhang W B, Bian L P *et al*. *Materials Science and Engineering A*[J], 2013, 585: 268

6 Zhang E L, Yang L. *Materials Science and Engineering A*[J], 2008, 497: 111

7 Srinivasan A, Huang Y, Mendis C L *et al*. *Materials Science and Engineering A*[J], 2014, 595: 224

8 Feyerabend F, Fischer J, Holtz J *et al*. *Acta Biomaterialia*[J], 2010, 6: 1834

9 Dai Y C, Li J, Yu L *et al*. *In Vitro Cellular and Developmental Biology-Animal*[J], 2002, 38: 373

10 Liu J, Yang L X, Zhang C Y *et al*. *Journal of Alloys and Compounds*[J], 2019, 782: 648

11 Zhang X B, Ba Z X, Wang Q *et al*. *Corrosion Science*[J], 2014, 88: 1

12 Zhang X B, Ba Z X, Wang Z Z *et al*. *Corrosion Science*[J], 2016, 105: 68

13 Zhang X B, Wu Y J, Xue Y J *et al*. *Materials Letters*[J], 2012, 86: 42

14 Yao H, Wen J B, Xiong Y *et al*. *Materials*[J], 2018, 11: 1564

15 Yao H, Wen J B, Xiong Y *et al*. *Journal of Alloys and Compounds* [J], 2018, 739: 468

16 Miao H W, Huang H, Shi Y J *et al*. *Corrosion Science*[J], 2017, 122: 90

17 Zhang J S, Zhang W B, Bian L P *et al*. *Materials Science and Engineering A*[J], 2013, 585: 268

18 He Z L, Fu P H, Wu Y J *et al*. *Materials Science and Engineering A*[J], 2013, 587: 72

19 Cao F Y, Song G L, Atrens A. *Corrosion Science*[J], 2016, 111: 835

20 Niu H Y, Deng K K, Nie K B *et al*. *Journal of Alloys and Compounds*[J], 2019, 787: 1290

21 Srikant G. *Corrosion Science*[J], 2012, 62: 90

22 Zhang Y, Li J Y, Liaw P K *et al*. *Journal of Alloys and Compounds*[J], 2018, 769: 552

23 Cao F Y, Shi Z M, Song G L *et al*. *Corrosion Science*[J], 2015, 90: 176

24 Ding Y F, Wen C, Hodgson P *et al*. *Journal of Materials Chemistry B*[J], 2014, 2: 1912

25 Li J H, Barrirero J, Sha G *et al*. *Acta Materialia*[J], 2016, 108: 207

26 Guan L, Zhou Y, Zhang B *et al*. *Corrosion Science*[J], 2016, 103: 255

27 Liu S J, Yang G Y, Luo S F *et al*. *Journal of Alloys and Compounds*[J], 2015, 644: 846

28 Chen J X, Tan L L, Yu X M *et al*. *Journal of Materials Science and Technology*[J], 2019, 35: 503

29 Xu D K, Liu L, Xu Y B *et al*. *Journal of Alloys and Compounds* [J], 2006, 426: 155

30 Akhtar A, Teghtsoonian E. *Philosophical Magazine*[J], 1972, 25: 97

31 Labusch R. *Physica Status Solidi A-Applications and Materials Science*[J], 1970, 41: 659

32 Bae D H, Kim S H, Kim D H *et al*. *Acta Materialia*[J], 2002, 50: 2343

33 Zhao Z Y, Bai P K, Guan R G *et al*. *Materials Science and Engineering A*[J], 2018, 734: 200

34 Ascencio M, Pekguleryuz M, Omanovic S. *Corrosion Science* [J], 2014, 87: 489

35 Yang L, Zhang E. *Materials Science and Engineering C*[J], 2009, 29: 1691

36 Lu Y, Bradshaw A R, Chiu Y L *et al*. *Materials Science and Engineering C*[J], 2015, 48: 480

37 Nordlien J H, Ono S, Masuko N *et al*. *Corrosion Science*[J], 1997, 39: 1397

固溶处理Mg-0.5Zr-1.8Zn-*x*Gd生物可降解镁合金的微观组织、力学性能和腐蚀性能

姚　怀[1,2]，熊　毅[1,2]，查小琴[3]，李　欢[1]，师慧娜[1]，刘　亚[1]

(1. 河南科技大学 材料科学与工程学院，河南 洛阳 471023)

(2. 有色金属共性技术河南省协同创新中心，河南 洛阳 471023)

(3. 洛阳船舶材料研究所，河南 洛阳 471000)

摘　要：研究了Mg-0.5Zr-1.8Zn-*x*Gd (*x*=0，0.5，1.0，1.5，2.0，2.5，质量分数，%) 镁合金经过470 ℃和10 h固溶处理后的组织、力学性能和耐腐蚀性能。结果表明，Gd含量在0%~2.5%范围内，随着Gd含量增加，合金晶粒尺寸逐渐减小。当Gd含量低于1.5%时，合金元素几乎完全固溶于合金基体中，第二相主要由纳米尺度的(Mg，Zn)$_3$Gd析出颗粒组成。当Gd含量在1.5%~2.5%范围时，合金中出现未固溶的微米尺度的(Mg，Zn)$_3$Gd相，并且该相数量和尺寸随着Gd含量增加而增加。由于组织均匀分布和纳米尺寸的第二相颗粒存在，Mg-0.5Zr-1.8Zn-1.5Gd合金具有优异的力学性能和耐腐蚀性能。在120 h浸泡实验中，Mg-0.5Zr-1.8Zn-1.5Gd合金平均腐蚀速率首先降低，然后增加，接着缓慢降低，最后，随着浸泡时间延长，腐蚀速率最终变得稳定。

关键词：镁合金；固溶处理；组织；力学性能；腐蚀

作者简介：姚 怀，男，1978年生，博士，讲师，河南科技大学材料科学与工程学院，河南 洛阳 471023，电话：0379-64231269，E-mail：yaohuai@163.com